Enhancing the catalytic performance of H-ZSM-5 in bio n-butanol dehydration by zeolite crystal engineering

Arno de Reviere, Jean-Pierre Gilson, Valentin Valtchev, Joris Thybaut, Maarten Sabbe, An Verberckmoes

Enhancing the catalytic performance of H-ZSM-5 in bio n-butanol dehydration by zeolite crystal engineering

Arno de Reviere[1,2], Jean-Pierre Gilson[3], Valentin Valtchev[3], Joris W. Thybaut[1], Maarten K. Sabbe[1,2], An Verberckmoes[2*]

[1]*Laboratory for Chemical Technology (LCT), Ghent University, Technologiepark 125, 9052 Ghent, Belgium.*

[2]*Industrial Catalysis and Adsorption Technology (INCAT), Ghent University, Valentin Vaerwyckweg 1, 9000 Ghent, Belgium.*

[3]*Laboratoire Catalyse et Spectrochimie, ENSICAEN, Université de Caen, CNRS, 6 Boulevard Maréchal Juin, 14050 Caen, France*

Abstract:

NH_4F etching is used as an unbiased chemical etching technique to hierarchize commercially available nano-sized ZSM-5 crystals. A structure-function relationship is reported, describing how the introduction of mesoporosity in a microporous ZSM-5 zeolite significantly increases its catalytic performance in (aqueous) n-butanol dehydration. Three parent samples are etched under two severity modes: mild (5 minutes of etching) and harsh (40 minutes of etching). Intrinsic features of the parent ZSM-5's, such as their silanol populations, influence the outcome of the etching procedure. For all materials, crystallinity is unaffected, total pore volume increases while micropore volume is almost constant, and active site accessibility increases. For all materials, etching increases the catalytic activity for n-butanol dehydration. Cofeeding water to n-butanol further increases the stability of all catalysts. Microkinetic modeling reveals that the increased activity is related to a decreased stability of dibutyl ether (DBE), the most abundant surface intermediate. A decreased DBE adsorption energy, due to the increased accessibility of the acid sites, facilitates its desorption. NH_4F etching, a flexible and easy technique to engineer zeolites' textural properties, does not affect the intrinsic nature and quantity of their active sites, leading to superior catalytic performances. Our results highlight the possibility to further increase the efficiency of zeolite catalysis in biomass conversion processes.

Keywords: NH_4F etching, hierarchization, H-ZSM-5, bio-butanol, aqueous butanol, butene, zeolite, microkinetic model

*Corresponding author: An Verberckmoes, E-mail address: An.Verberckmoes@ugent.be

1. Introduction

Transitioning towards a sustainable chemical industry requires a shift from fossil to renewable biomass-based resources and/or circular technologies [1-3]. The diverse approaches aim to efficiently convert renewable resources into valuable products, ranging from olefins and biofuels to platform chemicals [4, 5], thereby contributing to the sustainable utilization of biomass feedstocks. For instance, light olefins are and will remain a critical building block of the chemical industry, with a production volume of nearly 300 million tons per year [6-8]. Zeolites already play a key role in the production of light olefins [9-11] and are among the most important catalysts in the petrochemical industry, due to their chemical and thermal stability, ability to vary and control product distributions and tunable characteristics [12-15].

Zeolite micropores create a confined environment around their active sites that revolutionized many oil refining and petrochemical processes. However, this welcome benefit generates significant transport limitations on molecules with sizes congruent with the zeolite porosity, often referred to as configurational diffusion. The full potential of these active sites is, therefore, not always utilized. Facilitating the molecular transport throughout the crystals, by shortening the diffusion pathlength, allows to overcome such a drawback. A shorter diffusion pathlength is obtained by either a bottom-up approach, where nanometer-sized crystals are produced by direct synthesis [16], or by a top-down approach, where existing micron-sized zeolite crystals are modified by various chemical treatments. Both approaches produce so-called hierarchical zeolites with a network of interconnected micro- and mesoporosity [17]. Synthesis of nanosized zeolite crystals typically requires longer synthesis times and more complex procedures [18-23]. Nevertheless, some nanosized zeolites (*e.g.,* TS-1, UZM-14 [nano-MOR] [24, 25],…) are already used in petrochemical applications.

Top-down procedures, such as chemical etching, on the other hand, have been utilized since the commercial introduction of zeolites as catalysts [26]. However, these methods affect not only their textural properties but also the chemical composition (increases or decreases of Si/Al ratio impacting the acidic properties of the active sites). Acid leaching causes dealumination [27] and the extracted Al is removed from the zeolite while after steaming, the extra-framework Al remains inside the zeolite micro- or mesopores [28]; after caustic leaching both Si and Al are removed but as under these conditions Si species (silicates) are more soluble than Al (aluminates), the net result is a desilication of the parent zeolite [29]. The effectiveness of these methods depends on the parent zeolite Si/Al ratio, e.g. a high silica zeolite dissolves more severe under caustic conditions than a low silica zeolite [30]. Such methods are referred to as biased. NH_4F-etching, on the other hand, is a

recently developed unbiased chemical etching procedure [26, 31, 32], leaving the Si/Al ratio unchanged. NH_4F-etching allows to decouple textural and compositional properties, contrary to caustic or acid-leaching techniques [33]. An unbiased etching also provides additional benefits:
1) It is not limited by the Si/Al ratio of the parent zeolites as it dissolves the crystals independently of their composition by selectively attacking defects in zeolite crystals like grain boundaries, interfaces between intergrown crystals,.. [26]. 2) Microporosity is retained [34], leaving intact the shape-selectivity of the zeolite catalyst. This method has been applied to well-understood, laboratory synthesized materials and some commercially available zeolites [35].
Post-synthesis engineering of zeolite properties (acidity/basicity [36], electronic properties [37], porosity [38], morphology [39], confinement around the active sites [40] …), often referred to as zeolite crystal engineering, is a major tool to fine-tune their performances in adsorption and catalysis. In the emerging field of biomass conversion, alcohol dehydration plays a key role. Bio-based alcohols are currently being produced on an industrial scale by fermentation, and associated downstream processes convert them to their corresponding alkenes [41]. While ethanol dehydration has been studied extensively [26, 42, 43], n-butanol dehydration is worth investigating for multiple reasons: 1) it is the most simple alcohol for which multiple alkene isomers can be formed and their ratio at low conversion reveals features of the active sites [44]. 2) Dibutyl ether (DBE) is readily formed over different zeolite catalysts (MFI, FAU, MOR, FER, TON) [45, 46] and the DBE/butenes ratio can be linked to pore geometry at the active center and active site density [46]. In short, n-butanol dehydration allows to attribute catalytic performances to physicochemical properties of the zeolite material.

The exact consequences of modifications on zeolite catalysts are difficult to extract and often remain unclear, as multiple properties are affected simultaneously. It is for instance near impossible to associate the altered performance of a zeolite to changes at the active site level [47] as transition state energies, adsorption stabilities, generation of new and different active sites [48, 49], diffusional effects could play a role to various extents. Furthermore, differences in behavior are also a function of the reaction mechanism itself. This makes unraveling property-function relationships a non-trivial task.

In this work, properties of commercially available ZSM-5 zeolite crystals are engineered by NH_4F etching, introducing secondary mesoporosity without affecting the active site itself. To highlight the catalytic consequences of NH_4F chemical etching and obtain a quantitative structure-property-function relation, we have studied the dehydration of n-butanol over a series of 9 zeolite catalysts: 3 commercially available H-ZSM-5 (MFI topology) parents with Si/Al = 15, 25 and 40 and their NH_4F

etched derivatives under two different severities (etching times 5 and 40 minutes). Microkinetic modeling is used to relate the catalytic properties with the reaction mechanism.

2. Methodology

2.1 Catalyst preparation

2.1.1 Ammonium fluoride etching

Three commercial NH_4^+-ZSM-5 zeolites from Zeolyst are used as parents: MFI15 (CBV 3024E, Si/Al = 15), MFI25 (CBV 5524G, Si/Al = 25),and MFI40 (CBV 8014 with a Si/Al = 40).

NH_4F crystals (Sigma Aldrich), are dissolved until a clear 40 wt% NH_4F aqueous solution is obtained, prior to every treatment. The experimental conditions to produce derivatives of the above parents are: liquid/solid ratio is 40 g/g, the etching time is 5 or 40 minutes, the temperature is fixed at 25°C in an oil bath. After etching, the zeolite is recovered by filtering over cellulose filter paper and washed at least 4 times with 90°C distilled water, so that no residual fluorine is present [50]. All samples are dried at 60°C overnight before and after treatment. Table 1 summarizes the codes attributed to the parent zeolites and their derivatives together with their respective etching conditions. The etching yield is defined as the relative amount of dry zeolite retained upon etching.

Table 1. Zeolite catalysts studied in this work, NH_4F etching conditions, and material yield upon etching.

Sample[a]	Etching time (minutes)	Etching temperature (°C)	Liquid/solid ratio (g/g)	Yield (%)
MFI15	/	/	/	/
MFI15-25-05	5	25	40	75
MFI15-25-40	40	25	40	68
MFI25	/	/	/	/
MFI25-25-05	5	25	40	77
MFI25-25-40	40	25	40	68
MFI40	/	/	/	/
MFI40-25-05	5	25	40	80
MFI40-25-40	40	25	40	65

[a]Coding: MFIx-y-z: MFI zeolite with x: Si/Al ratio – y: etching temperature – z: etching time

All zeolites, are calcined under a constant and dry airflow (100 L/h) at 823 K for 4 h, with a heat ramp of 1 K min^{-1} to produce acidic (H^+) zeolite catalysts. They are further pelletized and sieved and the 75-100 µm fraction is retained for catalytic testing. The retained zeolite is then stored in a drying oven at 393 K until collected for catalytic testing.

2.2 Catalyst characterization

Surface area and pore volume are determined by N_2 physisorption at 77 K (Micromeritics Triflex). The samples are degassed under vacuum at 573 K for 6 hours prior to measuring. The BET area is calculated applying Rouquerol's criteria [51], and the external surface area from the t-plot method [52]; micropore volume and pore size distributions are determined using the non-local DFT method, assuming cylindrical pores [53]. X-ray diffraction (XRD) assesses whether any crystallinity or structural changes occur through the etching procedure. All FTIR measurements are performed on a Nicolet 6700 spectrometer. FT-IR spectroscopy of the dehydrated zeolite reveals acid sites and silanol groups. The pyridine adsorption is monitored *in-situ* by FT-IR to quantify the Brønsted and Lewis acid sites. The amount of acid sites is calculated after desorption at 423 K from areas of the bands at 1454 cm^{-1} (Lewis) and at 1545 cm^{-1} (Brønsted). Prior to FTIR analysis, the samples are pressed into 2 cm^2 self-supporting wafers and degassed in-situ overnight at 723 K under vacuum. The FTIR spectra/areas are normalized to a pellet density of 10 mg/cm^2 and the extinction coefficients are: $\varepsilon(B)_{1545}$=1.02 and $\varepsilon(L)_{1454}$ = 0.89 cm mol^{-1} [34, 54]. Si and Al elemental analysis is performed by ICP-OES to determine the Si/Al ratio. By calculating the ratio of Brønsted acid sites over amount of Al, an acid site accessibility parameter is obtained [55]. Solid-state ^{27}Al NMR spectra are recorded on a Bruker Avance III-500 spectrometer, the powder samples are introduced into a 4 mm Zr rotor to perform MAS experiments, using a spinning speed of 14 kHz. The chemical shifts are referenced to a 1M $Al(NO_3)_3$ aqueous solution. Transmission electron microscopy (TEM, JEOL JEM-2200FS) images are obtained to visualize the hierarchization.

2.3 Catalytic testing

The catalysts are tested in a high-throughput setup [44, 46]; the reactor tubes have a length of 0.8 m and an internal diameter of 2.2 mm. All catalysts are diluted with inert α-Al_2O_3 in a 1/10 catalyst/inert ratio to avoid hot and cold spots. Liquid n-butanol (>99.5%, Merck, hereinafter referred to as BuOH) or an aqueous BuOH solution (80/20 BuOH/H_2O mass ratio) are the feeds used throughout this work. The feed composed of 80/20 BuOH/H_2O is a saturated BuOH solution, which is used to represent a bio-butanol stream, *i.e.,* the mixture contains the maximum amount of water soluble in BuOH at room temperature [56]. Nitrogen (Air Liquide) is the carrier gas to regulate the inlet partial pressure of BuOH. The calcined and dried (*i.e.*, kept at 120°C before use) catalyst is loaded inside the reactors, heated to reaction temperature and kept for at least 4 hours under a steady N_2 flow of 10 Nl/hr. Downstream of the reactor section, all piping is heat traced at 433 K. The reactor effluent is analyzed by GC-FID, with ethane as the internal standard. All material balances in

this work close within 5%. Literature correlations indicate no mass transfer limitations under such experimental conditions [57].

The inlet partial pressure of BuOH is kept at 29 kPa in all experiments, as in previous work [21, 44, 46, 58]. To compare the catalysts on an active site basis, turnover frequencies (TOF) are calculated as follows:

$$TOF = \frac{F^0_{BuOH} - F_{BuOH}}{W * C_a}$$

with: F^0_{BuOH} the inlet flowrate of BuOH (mol s^{-1}), F_{BuOH} the outlet flowrate of n-BuOH (mol s^{-1}), W the mass of catalyst (kg), and C_a the active site density (amount of Brønsted acid sites in the catalyst in mol kg^{-1}). All reported TOFs are calculated at conversions, X_{BuOH}, below 25%, as:

$$X_{BuOH} = \frac{F^0_{BuOH} - F_{BuOH}}{F^0_{BuOH}}$$

To compare the catalytic activity over a broader conversion range, the site time is varied; it is defined as:

$$\text{Site time} = \frac{W\ C_a}{F^o_{BuOH}}$$

Hence, independent of the feed (pure or aqueous BuOH), the site time is related to the amount of BuOH fed.

The selectivity of product i, S_i is:

$$S_i = \frac{b_i\ F_i}{c_{BuOH} F^0_{BuOH}}$$

with b_i the number of carbon atoms of effluent *i*, F_i the outlet molar flowrate of *i*, c_j the number of carbon atoms in the feed component BuOH (= 4).

2.4 Microkinetic modeling

To gain a more fundamental understanding of the catalytic materials, a microkinetic modeling approach is applied for the MFI25 series (MFI25, MFI25-25-05, and MFI25-25-40). The model used is based on DFT-based reaction mechanisms for the dehydration of n-butanol on H-ZSM-5 by John et al., [59, 60]. Gunst et al. evaluated and compared the DFT-based kinetic model with experimental data for commercial H-ZSM-5 zeolites [61]. This model has been extended in our group to other

zeolites (FER, TON, MOR) [45, 46]. For more details on the mechanistic aspects of the model and kinetic data, the reader is referred to these papers.

In this work, the microkinetic model is utilized to understand how the chemical etching procedure affects the surface chemistry at a molecular level. Furthermore, the kinetic modeling approach allows quantification of the occurring effects.

All simulations are performed with python3, catalytic activities and selectivities are simulated, solving the microkinetic model as a function of reaction conditions in a plug flow reactor model. The reactor model is necessary to allow assessment of the effect of a realistic build-up of product pressures. This is necessary to calculate meaningful turnover frequencies (TOFs), that allow comparison with experimental results. Without consideration of the product pressures, no re-adsorption or equilibrium setting is allowed. Continuity equations are applied for the gas-phase components *i* and surface species *k* along with a site balance to determine individual turnover frequencies (TOFs), coverages (θ) and overall rates (R_i):

$$\frac{dF_i}{dW} = R_i = C_a \sum_j v_{ji} TOF_j \text{ , with } \mathrm{F}_i = \mathrm{F}_{i,0} \text{ at } \mathrm{W} = 0 \quad (1)$$

$$\frac{d\theta_k}{dt} = \sum_j v_{jk}\, TOF_j = 0 \quad (2)$$

$$\theta^* + \sum_k \theta_k = 1 \quad (3)$$

where TOF_j is the turnover frequency of elementary step *j* (mol mol_{sites}^{-1} s^{-1}), v_{ji} the stoichiometric coefficient of component *i* in the elementary step *j*, θ_k the fractional coverage of surface species *k* (mol mol_{sites}^{-1}), θ^* the fractional coverage of free acid sites (mol mol_{sites}^{-1}), C_a the concentration of Brønsted acid sites (mol_{sites} kg^{-1}), F_i the molar flow rate of gas-phase component *i* (mol s^{-1}), *W* the mass of the catalyst (kg) and R_i the net production rate of gas-phase species *i* (mol kg^{-1} s^{-1}). This set of equations was solved numerically using the LSODA module of ODEPACK [62].

3. Results and discussion

3.1 Physicochemical characterization

All parent zeolites (MFI15, MFI25 and MFI40) display a type I isotherm (Figure S1) of a microporous zeolite, but with some minor mesoporosity as well. Comparing the parents to their etched

derivatives (Figure 1), it is noticeable that the mesopore fraction depends on etching time and the MFI25 series shows the lowest increase in mesopore volume.

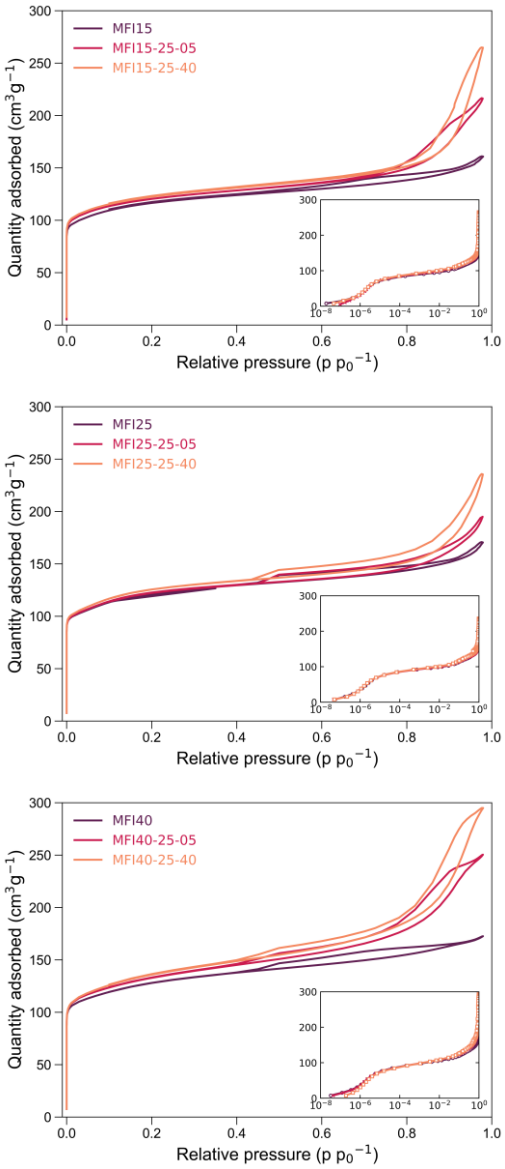

Figure 1. Nitrogen sorption isotherms of the MFI15, MFI25 and MFI40 series; insets are semi-log plots of the isotherms.

From the sorption isotherms, and their analysis, microporosity is hardly affected by the etching procedure. The nitrogen uptakes at low relative pressures are almost identical, and the resulting micropore volumes (V_{micro}) and micropore areas (S_{micro}) vary barely upon etching (Table 2). The total pore volume, on the other hand, nearly doubles for the MFI15 and MFI40 series. The increasing pore volume, together with the BJH pore size distributions (Figure S2), shows that with increasing etching time, both the amount of mesopores and their pore width increase (> 40 nm).

Table 1. Textural characteristics of the parent zeolites and their etched derivatives (N_2-physisorption)

Sample	V_{micro} (cm^3/g)	V_{tot} (cm^3/g)	S_{BET} (m^2/g)	S_{micro} (m^2/g)	$S_{meso+ext}$ (m^2/g)
MFI15	0.167	0.248	428	382	46
MFI15-25-05	0.161	0.333	446	380	66
MFI15-25-40	0.167	0.407	454	388	65
MFI25	0.176	0.263	441	395	46
MFI25-25-05	0.172	0.298	444	393	50
MFI25-25-40	0.178	0.366	460	399	61
MFI40	0.184	0.265	469	413	56
MFI40-25-05	0.162	0.385	485	375	110
MFI40-25-40	0.163	0.455	491	376	115

TEM analysis is used to visualize the secondary porosity. NH_4F etching first dissolves the zone of structural stress at the interface of twins or randomly intergrown crystals [63]. Going deeper in the crystal volume, the interfaces between misoriented grain boundaries are dissolved, generating rectangular mesopores [26]. This dissolution mechanism is characteristic of any zeolite subjected to a fluoride medium etching. However, the particularities of the dissolution process are more difficult to observe in the case of nanosized and heavily intergrown crystals. Similarly to the micron-sized crystals the nanosized samples in this study are dissolved along the planes of intergrowth. This divides the material into very small nanocrystals, connected by mesoporous cavities. TEM images, Figure 2, indicate that the nature of the mesoporosity is different for the MFI25 series compared to the MFI15 and MFI40 series. The MFI15 and MFI40 series mesopores appear as cut aggregates, allowing disassembly into smaller nanocrystals. A lot of tiny cavities are already present in the parent MFI40 zeolites compared to the MFI15 parent zeolite; which increases the external surface area. Together with MFI40 being the most intergrown of the studied parent materials, this is probably why it is the most responsive to NH_4F etching, a kinetically controlled step. The higher responsiveness of MFI40 to the etching procedure likely causes the small decrease in microporosity (Table 2). Upon etching, the cuts in MFI15 and MFI40 start near the edges of the crystal aggregates and follow a straight line to the center. Straight cuts or “cracks” obtained upon NH_4F etching have already been observed before for MOR-crystal aggregates [64]. These straight cuts follow the intergrowth interface and reveal information on the crystallization history. Seeding was probably used in the preparation of this industrial sample. At saturation concentration and with many nuclei, intergrowth formation is enhanced in the parent MFI15 and MFI40 zeolites. Hence, the ubiquitous intergrowth areas observed for these crystals where the cracks can be initiated [65]. For the supplied MFI25 parent, the crystals are more perfect, less aggregated and less intergrown. As a result, more intra-

particle mesopores with straight edges are therefore obtained upon etching. These types of mesopores have been linked to the mosaic structure of the zeolite crystals [31], where small nano-domains are dissolved during the etching procedure. Overall, the outcome of the etching procedure on MFI zeolite samples is largely dictated by the crystallization or manufacturing procedure and the resulting properties of the parent zeolite. Consequently, a 'perfect zeolite' without defects or intergrowths would be the least responsive to NH_4F etching.

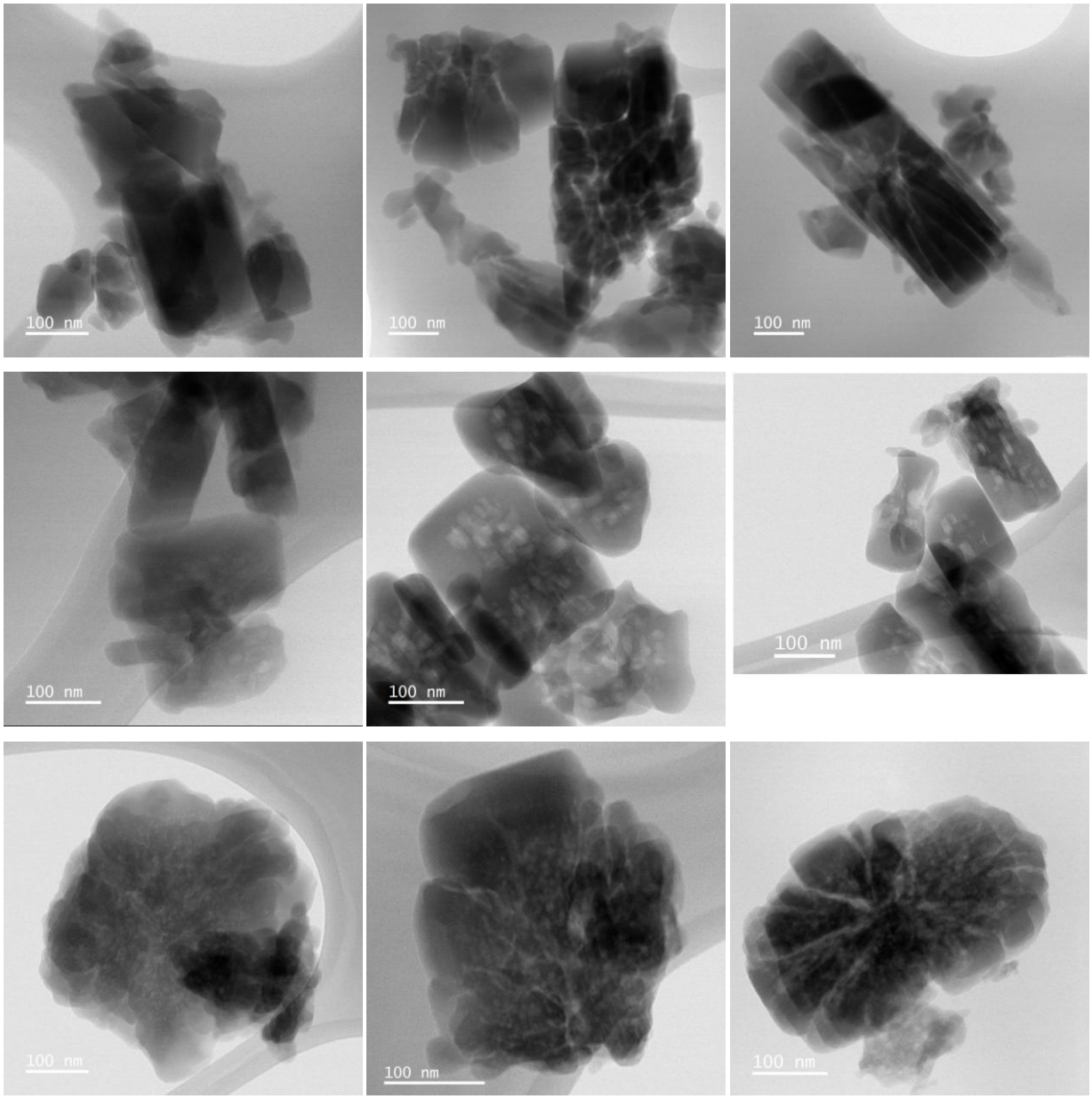

Figure 2. TEM images of the zeolite crystals used in this work. From left to right: parent – sample after 5 minutes of etching – sample after 40 minutes of etching. From top to bottom: MFI15 – MFI25 – MFI40 series.

The concentration of Brønsted and Lewis acid sites measured by pyridine-FTIR on the various zeolites is summarized in Table 3.

Table 2. Amount of Brønsted acid sites, Lewis acid sites (Py-FTIR), Si/Al ratio (ICP-OES) and H^+/Al (Py-FTIR + ICP-OES) for the series of catalysts

Sample	C_B (µmol g^{-1})		C_L (µmol g^{-1})		C_{tot} (µmol g^{-1})		Si/Al	H^+/Al
	423 K	523 K	423 K	523 K	423 K	523 K		
MFI15	565	506	169	128	744	633	15.3	0.55
MFI15-25-05	536	444	139	95	675	539	19.8	0.67
MFI15-25-40	615	513	204	140	819	652	20.4	0.79
MFI25	335	267	57	64	392	331	28.5	0.59
MFI25-25-05	367	307	87	90	455	397	29.0	0.66
MFI25-25-40	423	360	109	72	532	432	28.4	0.75
MFI40	314	237	87	60	401	297	42.3	0.82
MFI40-25-05	236	206	77	58	312	264	41.4	0.60
MFI40-25-40	247	212	111	81	358	292	38.4	0.58

Silanol groups are also present in the different samples (Figure 3). The sharp peak at 3745 cm^{-1} corresponds to external silanols, located on the external surface and edges of the crystals [66]. The intensity of the band characteristic of Brønsted acid sites at 3610 cm^{-1} is greater for lower Si/Al ratios. The band at 3664 cm^{-1} indicates the presence of extra-framework Al generating Lewis acidity [50, 67]. MFI15 clearly has the most intense band at 3664 cm^{-1}, thus the most extra-framework Al, in agreement with Rodriguez-Gonzalez et al., where a lower Si/Al ratio for MFI zeolites was linked to higher amounts of extra-framework Al [68]. The broad IR band (3500-3100 cm^{-1}) is due to internal silanol nests [69], which originate from a missing T atom in the framework [70]. This indicates that MFI25 possesses the lowest amount of silanols, hence, its lower sensitivity to chemical etching. Furthermore, it has the lowest amount of Lewis acid sites of all parent zeolites (measured at 423 K). For all derivatives, the intensity of the band at 3745 cm^{-1} increases upon etching (Figure S3), due to the increased external surface [34]. The broad band ascribed to internal silanol nests decreases upon etching, just as the intensity at 3664 cm^{-1}, related to extra-framework Al, highlighting again that etching preferably attacks weak spots (often referred to as defects) in zeolites.

MFI40 has a higher number of Lewis acid sites than MFI25 at 423 K, probably due to some dealumination during its processing on a large scale. Dealumination could also explain why MFI40 has the highest initial mesoporosity and its higher reactivity to chemical etching. This is also corroborated by ^{27}Al NMR, where MFI40 clearly has the most Al(VI). After etching, all materials have a decreased peak at 0 ppm (Figure S4 to S6), indicating fewer octahedral Al, as corroborated by the in-situ FTIR. Nevertheless, the MFI15 and MFI25 series show a broad signal between 45 and 10 ppm,

which might indicate extra-framework Al clusters in a less-organized extra-framework phase [71]. This signal is more pronounced for MFI15 and could explain why it is more susceptible to etching compared to MFI25, as the extra-framework Al can initiate the etching. None of the etched samples show an AlF_3 peak at – 20 ppm, indicating that the samples are thoroughly washed, leaving no residual fluoride species [72].

Oddly, the amount of available Brønsted acid sites decreases in the MFI40 derivatives, while accessibility is expected to increase after such a treatment. The total amount of acid sites measured after pyridine desorption at 250°C is almost identical for the treated and parent sample in the MFI40 series. This indicates that some of its extra-framework Al is more difficult to extract than framework Al and might be due to the presence of polymeric alumina species in the zeolite agglomerate.

Generally, the Brønsted acid site accessibility increases upon NH_4F-etching, but more Lewis acidic sites become available, indicating an increased accessibility of the present extra-framework Al. Furthermore, the susceptibility to chemical etching seems to be related to the amount of silanol defects present. The amount of external silanols increases due to the etching, and the amount of internal silanol nests decreases.

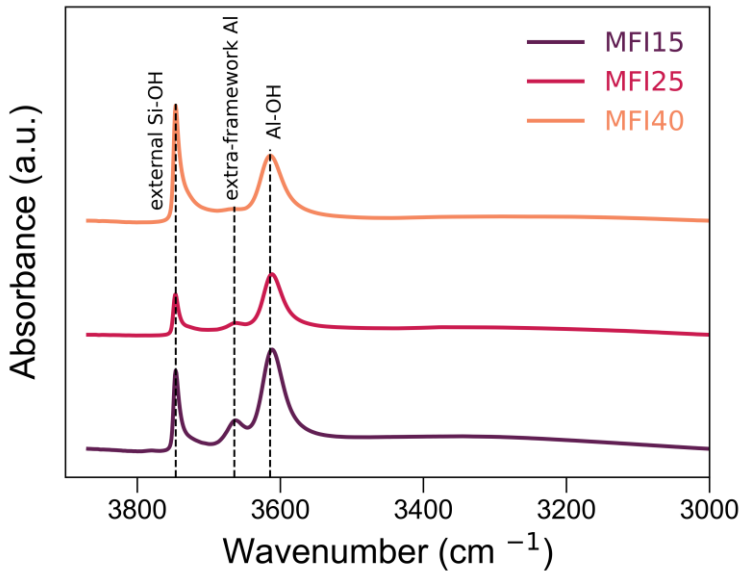

Figure 3. Normalized FTIR spectra in the OH-stretching region for the parent catalysts activated at 723 K.

3.2 Kinetic screening of n-butanol dehydration over hierarchized ZSM-5

A temperature screening is first performed on all zeolites to determine optimal conditions for a detailed kinetic evaluation (section 3.3). The TOF of n-butanol dehydration/conversion, depending on temperature, from 453 to 503 K, is shown in Figure 4. All TOFs are calculated at conversions below 25% and are normalized per Brønsted acid site.

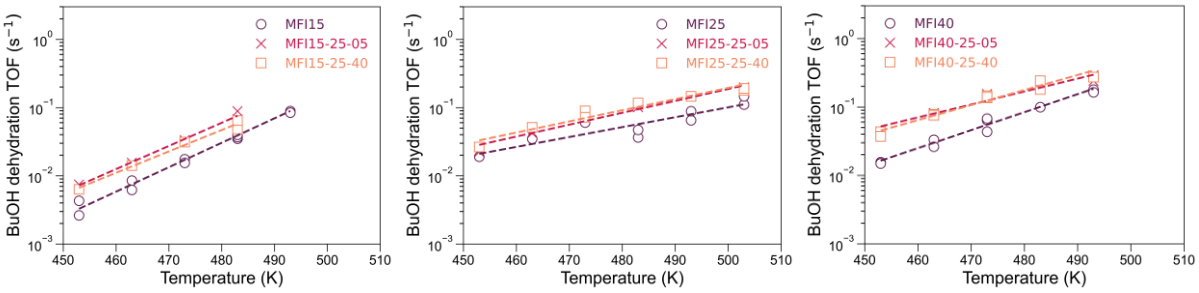

Figure 4. n-butanol turnover frequency (TOF) at conversions below 25% as a function of temperature for parent MFI zeolites (○), hierarchical derivatives etched for 5 minutes (×) and 40 minutes (□). The inlet partial pressure of n-butanol is 29 kPa, the total pressure is 5 Bar, the space time for all datapoints is approximately 5 kg s mol^{-1}.

The activity of all hierarchical zeolites is systematically higher than their parent. Moreover, in all three families of catalysts, the activity of hierarchical derivatives etched for either 5 or 40 minutes are identical. Nevertheless, the apparent activation energies are constant within 5 kJ mol^{-1} for each catalyst family; $E_{a,app}$ = 142-147 kJ mol^{-1} for the MFI15 series, 103-105 kJ mol^{-1} for MFI25 and 110-114 kJ mol^{-1} for the MFI40 series. Hence, the reaction chemistry and dominant reaction mechanisms remain unaltered. The activity of hierarchized zeolites on an acid site basis is higher compared to the parent material, probably due to enhanced accessibility of the acid sites. Yet, severe etching apparently does not further increase accessibility compared to mild etching. Hence, the activity upon deep etching is identical to the mildly etched zeolite, even though the amount of available acid sites to catalyze the dehydration reaction increases with etching time.

Based purely on activity data, the causes of the increased activity of the hierarchical derivatives are not evident: physical (enhanced diffusion) or chemical (energy barriers, surface coverages...). However, diffusional effects seem unlikely, as the zeolite crystals are nanosized, the reaction rates at 453 K are low, and the kinetics are considered intrinsic until much higher temperatures (and rates).

Another important measure of a catalyst is product selectivity. Especially for BuOH dehydration, it has been shown that the activity of a catalyst is strongly linked to the reaction pathways. Experimentally, different product selectivity is a simple measure to assess dominant reaction pathways. To this end, we have extended the experimental dataset for the activity measurements to assess the selectivity profile, Figure 5. The most interesting selectivity behavior is at lower conversions, as at higher n-butanol conversion levels, thermodynamic equilibrium between the butene isomers is set [58], independently of the Si/Al ratio [61] or framework topology [46]. Interestingly, for the MFI15 (Figure 5) and MFI40 (Figure S7) series, no selectivity effects are observed. Previously, Gunst et al. explained such a behavior of an increased activity without affecting selectivity by adsorption strength and active site coverage [61].

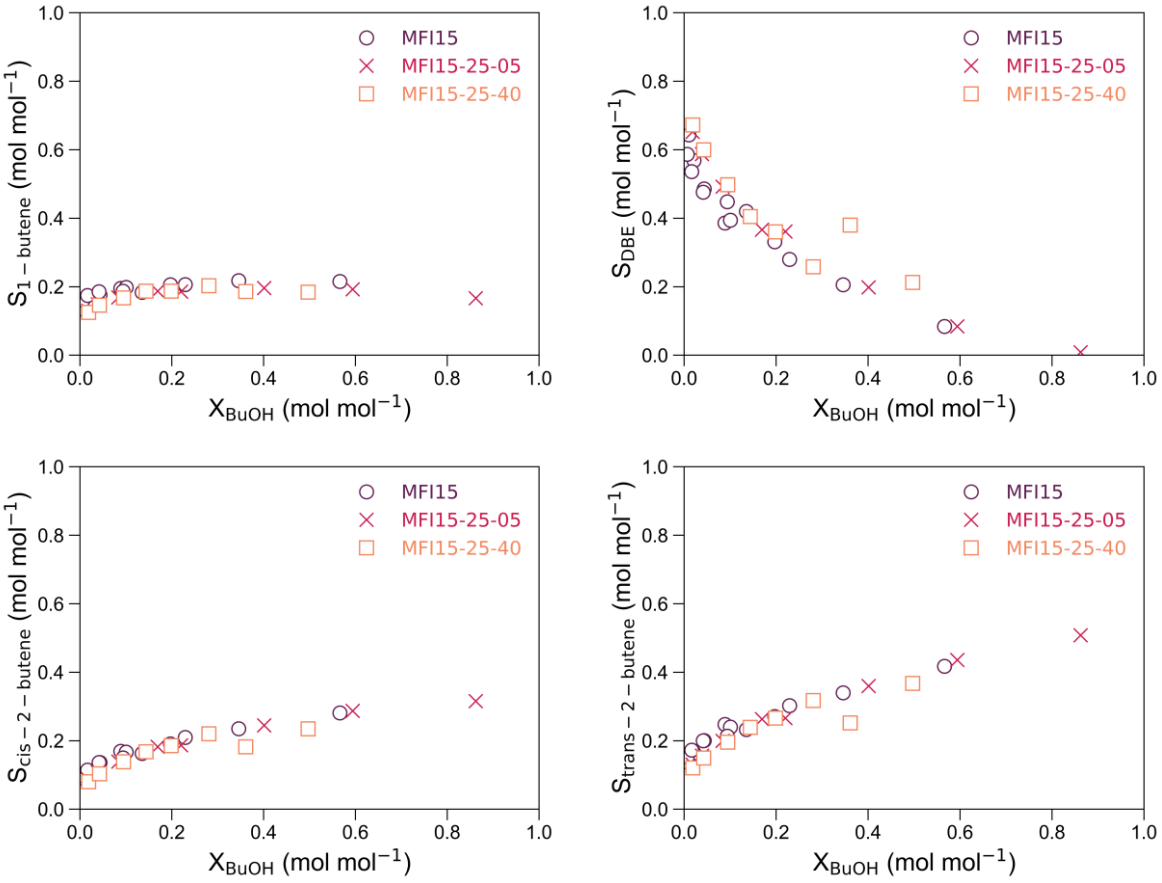

Figure 5. Selectivity of products during n-butanol dehydration over MFI15 (○), MFI15-25-05 (×) and MFI15-25-40 (□). Temperature ranges for MFI15 & MFI15-25-05: 453 – 513 K, for MFI25-25-40: 453 – 493 K, the inlet partial pressure of n-butanol is 29 kPa, the total pressure is 5 Bar, and the space-time for all datapoints is approximately 5 kg s mol^{-1}.

For MFI25, on the other hand, we see an increased selectivity to DBE compared to the butenes for the hierarchical materials compared to the parent material (Figure 6). This different behavior is somewhat unexpected when compared to the other series, nevertheless, MFI25 is also the material on which the etching procedure had a different effect compared to MFI15 and MFI40. Because of this different behavior, this set of materials is considered the most interesting for further investigation.

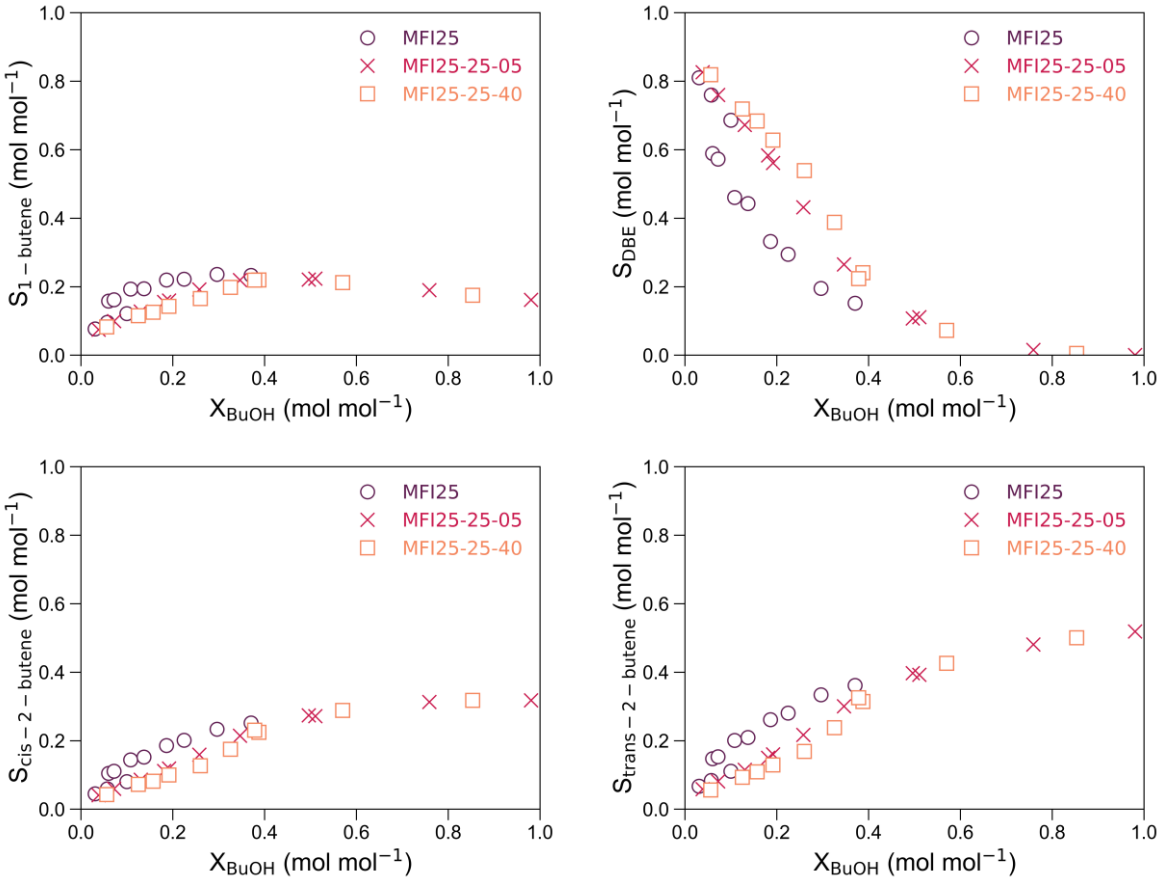

Figure 6. Selectivity of products during n-butanol dehydration over MFI25 (○), MFI25-25-05 (×) and MFI25-25-40 (□) for the temperature screening experiments (range MFI25: 453 – 513 K, MFI25-25-05: 453 – 533 K, MFI25-25-40: 453 – 523 K). The inlet partial pressure of n-butanol is 29 kPa, the total pressure is 5 Bar, the space time for all datapoints is approximately 5 kg s mol^{-1}.

The average number of interactions between the reagent and active site, N_{H+}, is defined by Khare et al. as the crystal size (in nm) divided by the Si/Al [73]. As the crystal size for the parent zeolites are similar, changes in selectivity have to be related to the number of interactions a reactant can have with acid sites in the microporosity. As the DBE selectivity decreases with increasing Al in the crystal (or decreasing Si/Al ratio), isomerization is facilitated; the DBE formed is promptly decomposed in the micropores of the low Si/Al ratio zeolites. Variations in selectivity due to a different Al content per crystal were already observed by Khare et al. for MTO in H-ZSM-5 [73]. Overall, these results are specific to the MFI25 series and could be linked to textural properties. In the MFI15 and MFI40 series, only cuts appear in the crystal aggregates leaving the molecular pathlength in the micropores almost unaltered. Hence, apart from the cuts in the zeolite crystals, the etched zeolite aggregates remain similar to the parent crystals. The MFI15 and MFI40 derivatives behave as their parent, but the overall activity is increased. Variable activity, without a change in selectivity, has been observed before and explained by a different active site occupation due to changes in overall adsorption strength [61]. Next to adsorption effects, the increased activity is likely related to a better

accessibility of the active sites upon etching. The increased accessibility of the acid sites is due to: (i) the secondary porosity reduces the pathlength of the molecules in the micropores, and acid sites that were inaccessible prior to etching are now exposed. (ii) The internal silanol nests are removed upon etching (Figure S3), whilst these can act as a trap for molecules and coke precursors [69, 74], which could block acid sites. Li et al. observed that for two ZSM-5 samples with similar physicochemical properties apart from silanol nest content, the activity for furfuryl alcohol etherification is noticeably higher for the sample with low silanol nest content [75].

The etched MFI25 derivatives, on the other hand, behave as smaller crystals as rectangular blocks are removed from their parent. This increases the number of pore mouths and leads to higher conversion [76]. To validate this hypothesis, catalyst stability is monitored in section 3.4, as an increased amount of pore mouths and hierarchization is correlated to a more stable catalyst. This increased activity and change in selectivity for MFI25-25-05 and MFI25-25-40 requires more in-depth analysis and is the focus of the next sections.

3.3 Kinetic evaluation of MFI25 series for bio-alcohol dehydration

3.3.1 n-butanol dehydration

An in-depth kinetic evaluation of the MFI25 series is essential to assess structure-property-function relationships. It takes place at two temperatures (483 and 513 K) for the parent and its two derivatives. The conversions are reported in Figure 7.

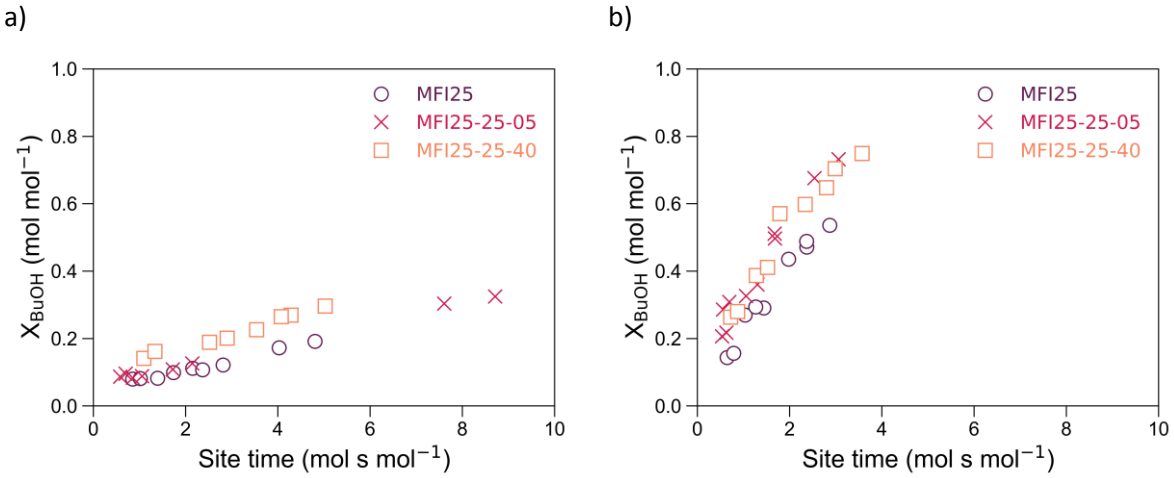

Figure 7. n-butanol conversion (X_{BuOH}) as a function of site time for MFI25 (○), MFI25-25-05 (×) and MFI25-25-40 (□). The inlet partial pressure of n-butanol is 29 kPa, the total pressure is 5 Bar, reaction temperature = 483 K (a), 513 K (b).

As in the temperature screening experiments, BuOH conversion on the etched catalysts is higher than their parent, and equal on an active site basis at 513 K. For BuOH dehydration, careful considerations are necessary to decouple activity and selectivity as the pathways towards the

different products vary in intrinsic activity. Thus, depending on the operating conditions (e.g., partial pressure of n-butanol), the activity can differ as the dominant reaction pathways shift, leading to both a different activity and selectivity. Therefore, the activity analysis is coupled with a selectivity analysis. At 483 K (Figure S8), the selectivity towards DBE is higher over the etched zeolites at the cost of selectivity towards the 2-butenes. The mechanistic basis for this behaviour is discussed in section 3.5, in which we propose that the behaviour could be related to a decreased surface stability of DBE* on the etched derivatives. The increase in activity is partly explained by an increased active fraction of the acid sites. At 483 K, MFI25-25-05 behaves intermediately between the parent sample and MFI25-25-40, this allows zeolite crystal engineering to steer the activity and product distribution.

However, at 513 K, this difference in selectivity between the parent and etched samples seems to disappear (Figure 8), while the activity difference remains. This indicates that enhanced diffusion of bulky DBE in the mesopores is not the cause for an increase in activity; the DBE selectivity difference between the parent MFI25 and etched derivatives would otherwise appear with higher temperatures. The suppression of differences in selectivity at higher temperatures, is not completely unexpected. Under these higher temperature conditions, the selectivity approaches thermodynamic equilibrium at lower conversion levels compared to the lower temperature experiments. Nevertheless, at lower conversion levels, it is probable that the selectivity towards DBE and the 2-butenes could differ, however, due to the high activity for the etched materials, it is difficult to obtain such low conversions at 513 K. Ultimately, the active centers themselves remain unaltered upon etching, although their accessibility is enhanced. Therefore it is reasonable that the selectivity of the dehydration products remains largely unaffected at higher temperatures. Upon full conversion, when the secondary reaction (oligomerization, cracking,..) products become more important, selectivity differences are expected due to the size of these products involved. The formation of these secondary products is purposely suppressed to focus on the dehydration reaction itself by working at lower conversion conditions.

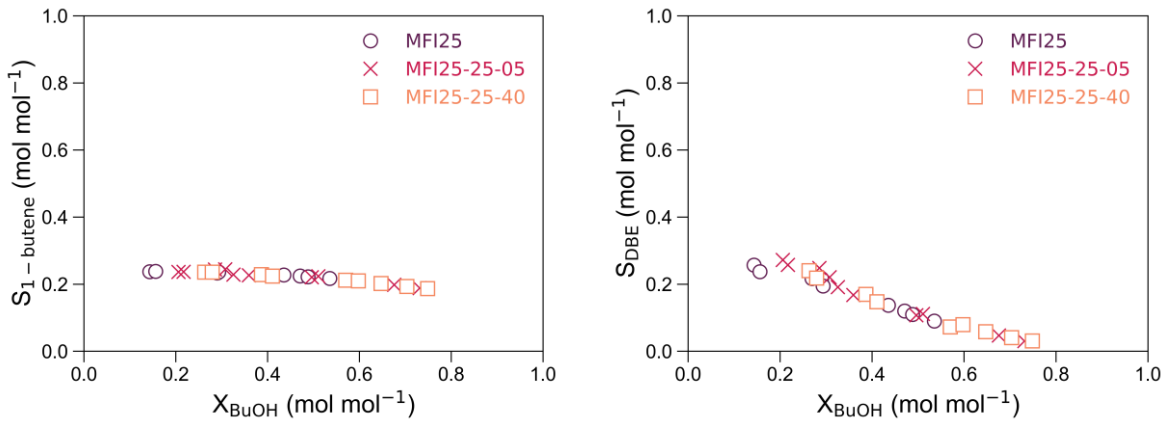

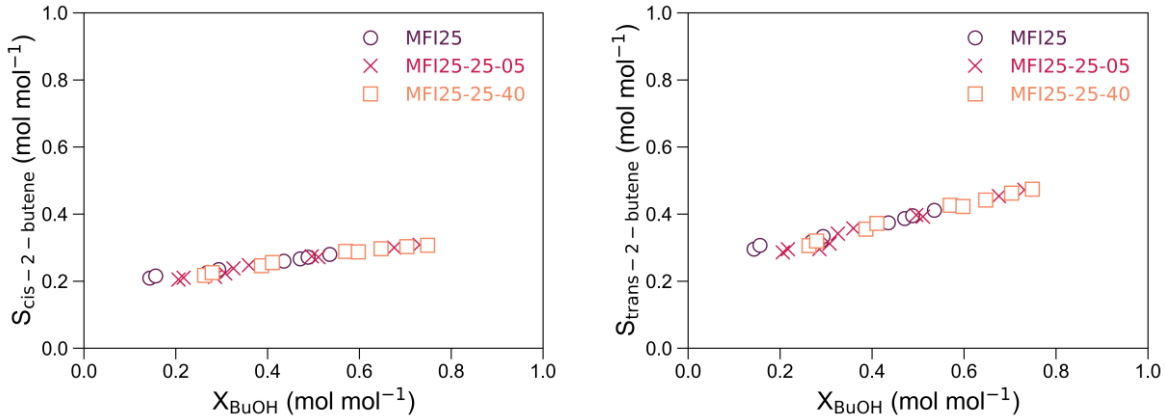

Figure 8. Selectivity of products during n-butanol dehydration over MFI25 (○), MFI25-25-05 (×) and MFI25-25-40 (□). The inlet partial pressure of n-butanol is 29 kPa, the total pressure is 5 Bar, the reaction temperature is 513 K.

The etching leads to increase in the activity without affecting the selectivity at higher temperature and conversion. This is essentially possible because the active site is not altered upon treatment. Therefore, etching the materials allows for overcoming activity/selectivity trade-offs at relevant operating conditions, which is very attractive from an industrial point of view.

3.3.2 Aqueous n-butanol dehydration

To investigate the performance of the zeolite catalysts for a bio-based alcohol stream, the effect of water in the feedstock is assessed. BuOH and water mixtures are only soluble in limited quantities; approximately 7 m% of BuOH in water and 20m% of water in BuOH [56]. Therefore, we have tested a saturated BuOH/H_2O mixture, where a feedstock is prepared with the maximum amount of water soluble in BuOH. Under the studied conditions, it is not expected that water has any effects on the structural stability of the studied zeolites [77], although at higher temperatures steaming could occur [28, 67]. The BuOH conversion at 513 K over the MFI25 and etched derivatives for both a pure and aqueous feed is shown in Figure 9, these results illustrate that the activity is not affected by cofeeding water; the conversion as function of site time is unaltered for all catalysts whether a pure or aqueous BuOH feed is used. Similar observations have been reported earlier [58, 78, 79]. The DFT-computed adsorption energy of n-butanol is much higher than that of water [60, 79], hence cofeeding water will not affect the surface coverage substantially. The activity results indicate no change in reaction mechanism, as the reaction rate is unaffected, as proposed by John et al. based on DFT-predicted reaction networks [60, 79]. Nevertheless, a selectivity analysis is required to confirm the absence of water effects on the reaction mechanisms, vide infra.

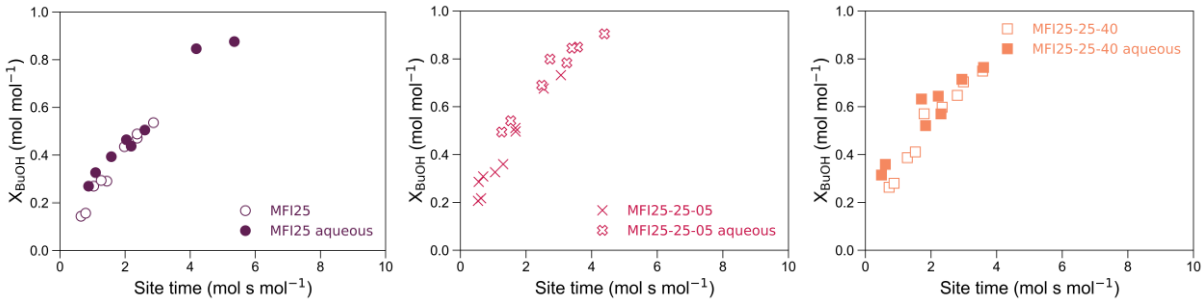

Figure 9. n-butanol conversion (X_{BuOH}) as a function of site time for MFI25, MFI25-25-05 and MFI25-25-40 for pure BuOH and aqueous BuOH feeds. The inlet partial pressure of n-butanol is 29 kPa, the total pressure is 5 Bar, reaction temperature is 513 K.

Similar as for a pure n-butanol feed, a selectivity analysis is performed, here the product selectivity over the zeolite catalysts for a pure and aqueous feed are compared for MFI25 (Figure 10), MFI25-25-05 (Figure S9) and MFI25-25-40 (Figure 11).

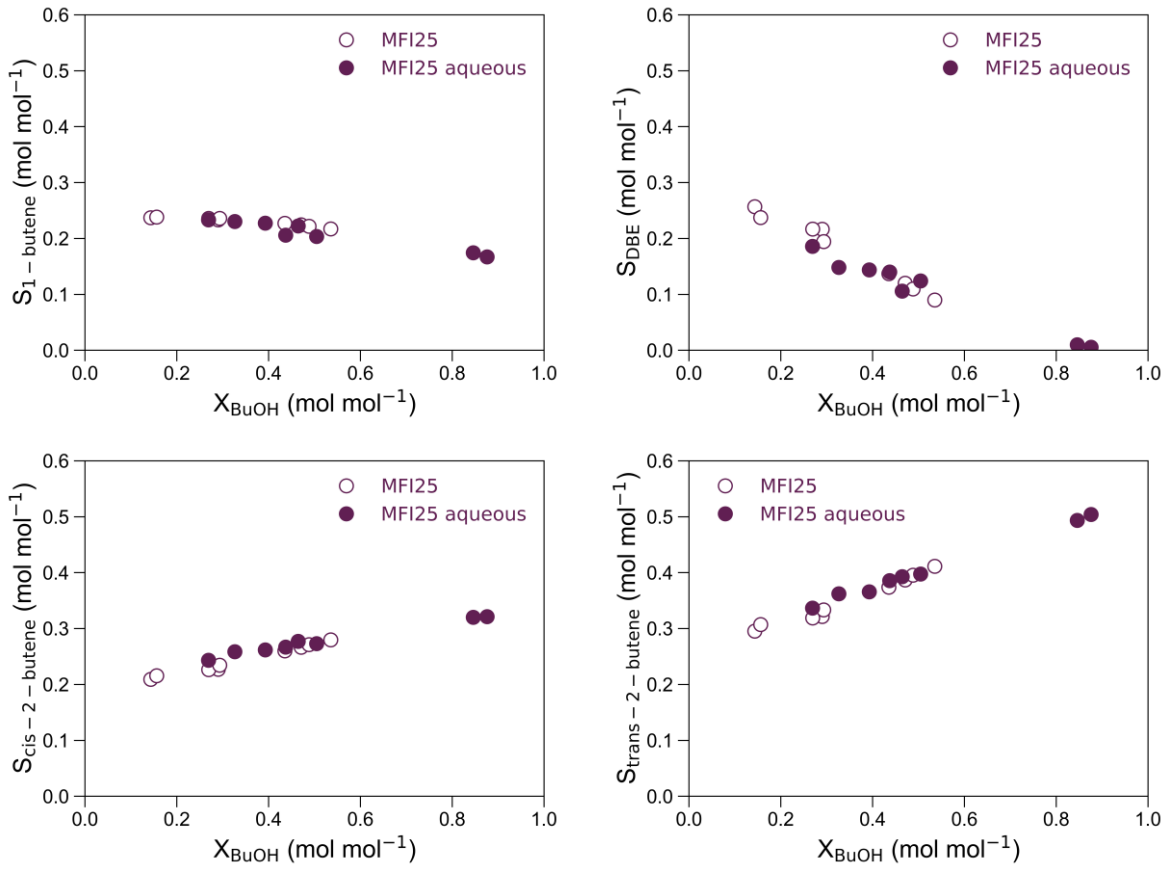

Figure 10. Selectivity of products during pure (hollow symbols) and aqueous (full symbols) n-butanol dehydration over MFI25. The inlet partial pressure of n-butanol is 29 kPa, the total pressure is 5 Bar, the reaction temperature is 513 K.

The selectivity of products does not differ significantly for an aqueous feed compared to a pure BuOH feed for the commercially obtained MFI25 zeolite. This corroborates that there is no change in

reaction mechanism upon cofeeding water, facilitating the processing of fermentation streams. For MFI25-25-05 (Figure S9) and MFI25-25-40 (Figure 11), similar results are obtained, where no noticeable effect on selectivity is observed. These results again indicate that the etching has no influence on the active site itself, as no noticeable effects are observed for either the parent and etched samples for both pure alcohol and aqueous feeds.

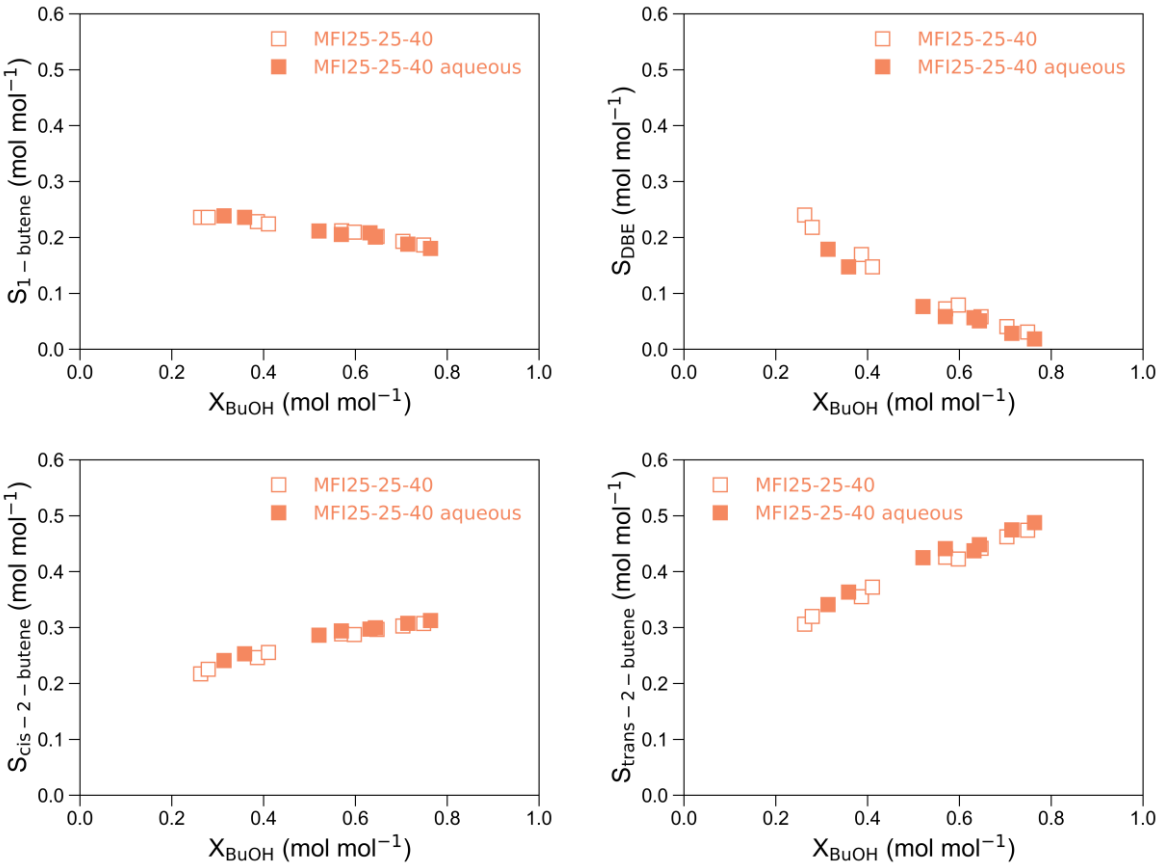

Figure 11. Selectivity of products during pure (hollow symbols) and aqueous (full symbols) n-butanol dehydration over MFI25-25-40. The inlet partial pressure of n-butanol is 29 kPa, the total pressure is 5 Bar, the reaction temperature is 513 K.

3.4 Catalyst stability for n-butanol dehydration on hierarchical ZSM-5

Next to activity and selectivity, the stability of the catalytic material is crucial to assess its performance. Therefore, the stability of MFI25, MFI25-25-05, and MFI25-25-40 is tested over a period of 60 hours for a pure BuOH feed (Figure 12, left) and an aqueous BuOH feed (Figure 12, right).

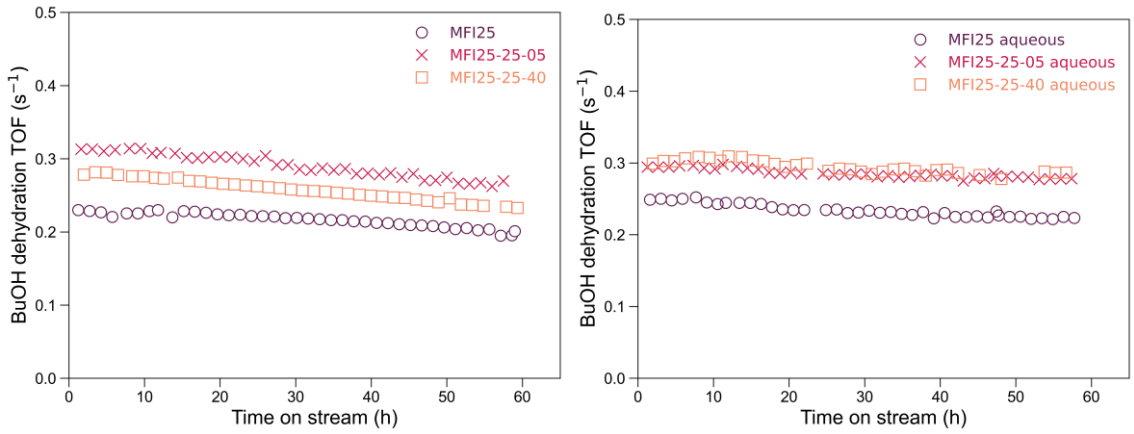

Figure 12. n-butanol (left) and aqueous n-butanol (right) conversion rates as a function of time for MFI25 (○), MFI25-25-05 (×) and MFI25-25-40 (□). The inlet partial pressure of n-butanol is 29 kPa, the total pressure is 5 Bar, the reaction temperature is 513 K.

For a pure BuOH feed, the etched materials show a more stable n-butanol conversion activity over time than their parent counterparts. An increased stability upon etching has been observed before [26, 76]. Nevertheless, it is remarkable that the etched materials are both more active and more stable. Typically, the more active the material, the less stable it becomes. For the etched zeolites this activity-stability trade-off has been overcome. Again, there is little difference noticeable between MFI25-25-05 and MFI25-25-40. The relative deactivation of MFI25 is 20%, where it is only 13% for MFI-25-25-05 and 15% for MFI25-25-40. Upon etching for only 5 minutes at the investigated conditions, the deactivation rate has been reduced by 35%, and the activity has increased by 60%. The reduced deactivation is explained by the materials behaving as smaller nanocrystals. Furthermore, as seen in section 3.1, upon etching the internal silanols were removed. Internal silanols have been linked to catalyst deactivation for other alcohol conversion studies (MTO, ETH) [26, 69] by retaining coke precursors at the internal defects [80]. Hence, coke is less prone to build up inside the micropores and is formed more on the external surface [81]. Coke formation is considered to have a smaller deactivating effect in the larger mesopores. Furthermore, the decreased adsorption strength of the strongest bound intermediate also leads to a lower deactivation.

Interestingly, the stability increases for all materials upon cofeeding water (Figure 12 left vs right), this effect is most noticeable for MFI25. This indicates that indeed internal silanols could be the cause of deactivation due to their ability to trap coke precursors [69, 74]. Cofeeding water has been shown to be able to sweep retained species from internal silanols [82] and decrease the deactivation rate of H-ZSM-5 for MTO. MFI25 has the most silanols and consequently its stability shows the strongest increase by cofeeding water. Another possibility could be that the cofed water influences (weakens or strongly adsorbs on) the strongest acid sites, where coke formation could otherwise initiate [83]. For aqueous feeds, the catalyst stability is nearly identical for all materials (relative

deactivations between 4 [MFI25-25-40] and 8 % [MFI25], hence within experimental error). It is not unlikely that this difference would increase for longer runs, giving a slight advantage to the etched materials.

3.5 Microkinetics of the n-butanol dehydration over hierarchized ZSM-5

To acquire new insights into the interesting behavior of the MFI25, MFI25-25-05 and MFI25-25-40 sequence, we performed a microkinetic modeling analysis (Figure 13; activity, Figure 14; selectivity at 513 K and Figure S10; selectivity at 483 K). The in-house developed microkinetic model for n-butanol dehydration is based on DFT calculations performed by John et al. [60, 79], which has been further extended over the years for other zeolite topologies [46], multiple Si/Al ratio's [61].

When comparing the behavior in the MFI25 series, the following differences are observed: (i) the activity is higher for both etched samples compared to the parent material, (ii) the selectivity to DBE increases slightly with etching time, similarly, the selectivity to 2-butenes is slightly lower for the etched materials. Therefore, the modifications to the microkinetic model should be limited preferably to 2 parameters, as there are only two important changes in behavior compared to the commercial material. All elementary reaction steps and corresponding kinetic and thermodynamic parameters are listed in Table S1.

The increased selectivity to DBE could be caused by an increased reaction rate towards the ether, e.g., by decreasing the energy barrier for ether formation. Another possibility is that the decomposition of the ether is suppressed over the etched materials, e.g., by an increased energy barrier for decomposition reactions. Changes in energy barriers imply that the zeolites are modified at an active site level, however, our experimental characterization indicates little to no effects to the active site itself. Therefore, it is probable that the additional mesoporosity and decreased internal silanols due to etching primarily affect the confinement near the active site. For large molecules, it is known that the interaction of the molecule with the zeolite framework is the primary contributor to adsorption energy rather than the acid site [84]. Furthermore, internal silanols can retain larger molecules (often related to coke formation [69, 74]), but also butanol [85] and DBE. Because DBE is larger, a stronger interaction with the internal silanols is expected. Thus, the confinement near the active site in turn, will influence the stability of large surface species, such as adsorbed dibutyl ether. From previous modeling studies for commercial H-ZSM-5 materials, we know that adsorbed DBE inhibits the catalytic activity for n-butanol dehydration [46, 61]. Decreasing the stability of adsorbed DBE on the acid site thus will lower the surface coverage of DBE, increasing its selectivity. Because adsorbed DBE is also the most abundant surface intermediate, a lower surface coverage of DBE (and hence facilitated DBE desorption) will lead to more available active sites, increasing the observed

activity. In this context, we have modeled the three materials of the MFI25 series, where only the adsorption enthalpy of DBE, ΔH_{ads}(DBE), has been altered for the etched materials.

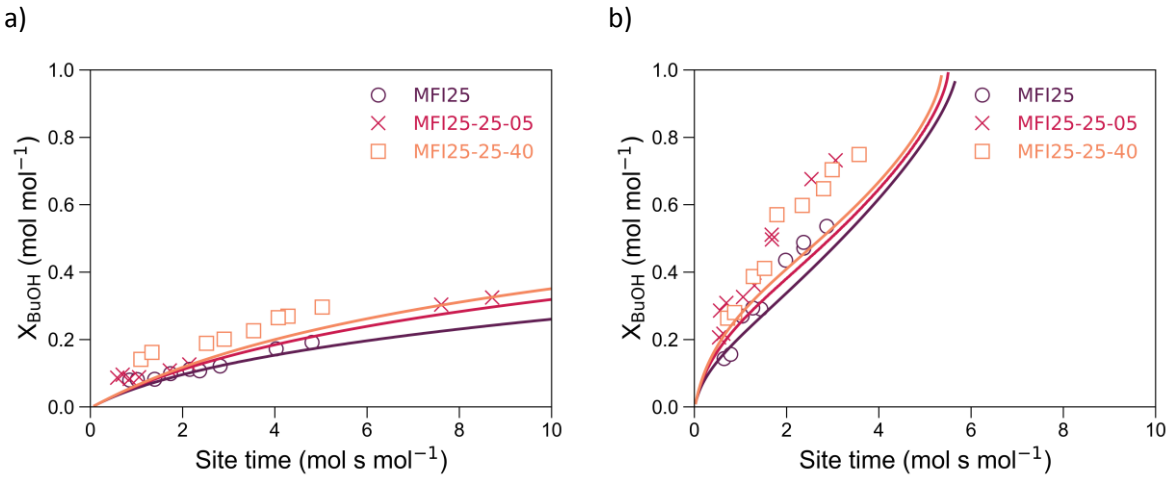

Figure 13. Experimental data (points) compared with model simulated results (lines) for the conversion of n-butanol as a function of site time over the MFI25 series at 483 K (a) and 513 K (b).

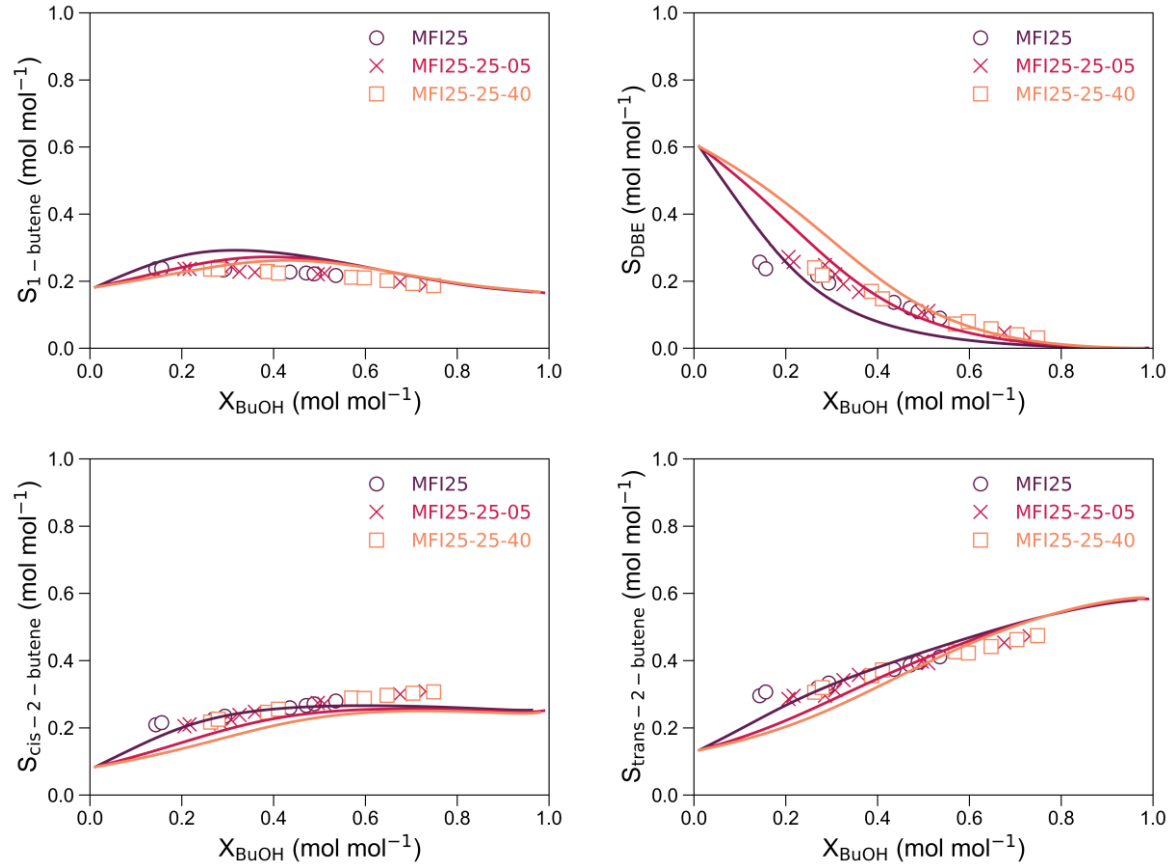

Figure 14. Experimental (points) and simulated (lines) selectivity of products during n-butanol dehydration over MFI25 (○), MFI25-25-05 (×) and MFI25-25-40 (□). The inlet partial pressure of n-butanol is 29 kPa, the total pressure is 5 Bar, the reaction temperature is 513 K.

As can be seen in Figures 13 and 14, the microkinetic modeling results agree relatively well with the three materials. More importantly, the trends are captured adequately: (i) the activity of the etched samples is significantly higher compared to the parent material but barely differs amongst one another, (ii) the difference in selectivity between the materials is more pronounced at 483 K (Figure S10) than at 513 K and decreases with conversion. Simulation results for an aqueous BuOH feed show no observable difference from a pure BuOH feed. This indicates that the surface stability of DBE could cause the marked increase in activity, with limited selectivity effects at 513 K. The DBE adsorption enthalpies are listed in Table 4.

Table 3. Changes in mesopore volume upon etching and resulting adsorption enthalpy of DBE.

Sample	V_{meso} ($cm^3\ g^{-1}$)	ΔV_{meso} ($cm^3\ g^{-1}$)	ΔH_{ads}(DBE) ($kJ\ mol^{-1}$)	$\Delta\Delta H_{ads}$(DBE) ($kJ\ mol^{-1}$)
MFI25	0.087	0	-217.6	0
MFI25-25-05	0.126	0.039	-214.9	2.7
MFI25-25-40	0.188	0.101	-213.6	4

Ultimately, the microkinetic modeling has allowed a quantified structure-property-function relation, where the additional mesoporosity and reduced, internal defects are related to a change in adsorption enthalpy for DBE.

4. Conclusions

In this contribution, an emerging and easy-to-use, unbiased NH_4F-etching to develop mesopores in commercial ZSM-5 zeolites is outlined. The etching is studied at room temperature for 5 and 40 minutes. The etching behavior of the parent zeolites and characterization of its derivatives provides valuable insights into the zeolite synthesis procedures. NH_4F-etching targets specifically intergrowths and point defects of the zeolites to create mesoporosity without affecting microporosity and overall composition (Si/Al). Such a treatment of the parent zeolites with Si/Al = 15 (MFI15) and Si/Al = 40 (MFI40) produces hierarchical zeolites in which the crystal aggregates are cut from the crystal edge towards the center. Another parent zeolite, Si/Al = 25 (MFI25), has a less aggregated structure and consists of more perfect crystals, and therefore, rectangular nano-domains are removed inside the crystals upon etching.

In the MFI25 series, the degree of etching impacts activity and selectivity at 483 K: for the mildly etched derivative these two properties are between its parent and the more severely etched derivative. This feature provides a textural property engineering of the zeolite. At higher temperatures, the zeolites etched for only 5 minutes display the same catalytic performance as those

etched for 40 minutes. This makes the etching procedure very efficient and allows for very short modification procedures. Only for the MFI25 series, there are selectivity effects noticeable upon treatment. These effects are clearly present at low temperatures and conversion, but thermodynamics dictates the selectivities at higher conversion. At higher temperatures, the conversion range for which selectivity effects are present decreases, thus, the etching procedure increases the activity but barely affects the selectivity. Cofeeding water shows no significant effects on BuOH dehydration rates. The experimental trends are captured with an in-house developed microkinetic model for n-butanol dehydration, which is extended toward the etched derivatives. The microkinetic analysis enables a mechanistic explanation for the observed behavior: the additional porosity and removal of internal silanol defects decrease the surface saturation by DBE*, increasing the observed activity. A quantified structure-property-function relation is therefore available. To the best of our knowledge, this is the first time that chemically etched zeolites behavior is described at such an elementary-step level. Future work could focus on in-situ DRIFTS studies, where the surface of the engineered zeolites is probed during reaction and the microkinetic model can be validated.

In addition, another key catalyst property, stability, is increased, circumventing traditional activity/stability tradeoffs. As the etching procedure has little effect on the active site, but may influence its near environment by removing some internal silanols, the absence of strong selectivity effects is reasonable for n-butanol dehydration. However, care should be taken for reactions where local confinement at the active site plays a crucial role in selectivity. Interestingly, for all zeolite catalysts, stability increases upon cofeeding water, yielding promising perspectives for bio-based alcohol streams. In conclusion, the NH_4F etching procedure offers a solution for various reactions where coke formation hinders zeolite performance.

A final word on the NH_4F etching procedure: the scale up to commercial scale of this procedure could present HSE issues due to the processing of fluorine containing streams. Such streams have been and are taken care of in a safe way in the processing of other zeolites, such as LZY-210; this zeolite first patented by Union Carbide (D.W. Breck, G.W. Skeels, US Patent 4,503,023 [1985] [86]) is a Y zeolite dealuminated with aqueous $(NH_4)_2SiF_6$ and commercialized by UOP after their acquisition of the Union Carbide zeolite business unit.

5. Acknowledgments

The calculations were carried out using the STEVIN Supercomputer Infrastructure at Ghent University, funded by Ghent University, the Flemish Supercomputer Center (VSC), the Hercules

Foundation, and the Flemish Government (department EWI). A.d.R. acknowledges the Research Foundation – Flanders (FWO) for the financial support through grant number V424220N. V.V. acknowledges the Industrial Chair Project n°CCR_ECOGAS2022 (TOTE: CT00000759-1).

6. References

[1] A.J. Ragauskas, C.K. Williams, B.H. Davison, G. Britovsek, J. Cairney, C.A. Eckert, W.J. Frederick, J.P. Hallett, D.J. Leak, C.L. Liotta, J.R. Mielenz, R. Murphy, R. Templer, T. Tschaplinski, The Path Forward for Biofuels and Biomaterials, Science, 311 (2006) 484-489.
[2] P.A. Willems, The Biofuels Landscape Through the Lens of Industrial Chemistry, Science, 325 (2009) 707-708.
[3] E.K.C. Moens, K. De Smit, Y.W. Marien, A.D. Trigilio, P.H.M. Van Steenberge, K.M. Van Geem, J.-L. Dubois, D.R. D'hooge, Progress in Reaction Mechanisms and Reactor Technologies for Thermochemical Recycling of Poly(methyl methacrylate), Polymers, 12 (2020) 1667.
[4] T. Vandevyvere, M.K. Sabbe, P.S.F. Mendes, J.W. Thybaut, J. Lauwaert, NiCu-based catalysts for the low-temperature hydrodeoxygenation of anisole: Effect of the metal ratio on SiO2 and γ-Al2O3 supports, Green Carbon, (2023).
[5] T. Vandevyvere, M.K. Sabbe, A. Bouriakova, S. Saravanamurugan, J.W. Thybaut, J. Lauwaert, Impact of the incipient wetness impregnation sequence during the preparation of La or Ce promoted NiCu-Al2O3 on low-temperature hydrodeoxygenation, Catalysis Communications, 181 (2023) 106734.
[6] H. Zimmermann, R. Walzl, Ethylene, Ullmann's Encyclopedia of Industrial Chemistry, Wiley-VCH Verlag GmbH & Co. KGaA, 2000.
[7] H. Zimmermann, Propene, Ullmann's Encyclopedia of Industrial Chemistry2013.
[8] N.V. Srinath, A. Longo, H. Poelman, R.K. Ramachandran, J.-Y. Feng, J. Dendooven, M.-F. Reyniers, V.V. Galvita, In Situ XAS/SAXS Study of Al2O3-Coated PtGa Catalysts for Propane Dehydrogenation, ACS Catalysis, (2021) 11320-11335.
[9] M.R. Gogate, Methanol-to-olefins process technology: current status and future prospects, Petroleum Science and Technology, 37 (2019) 559-565.
[10] P. Tian, Y. Wei, M. Ye, Z. Liu, Methanol to Olefins (MTO): From Fundamentals to Commercialization, ACS Catalysis, 5 (2015) 1922-1938.
[11] C.J. Stevens, P.A. Sechrist, I.R.A. Johnson, Two stage oxygenate conversion reactor with improved selectivity, Google Patents, 2016.
[12] A.F. Masters, T. Maschmeyer, Zeolites - From curiosity to cornerstone, Micropor Mesopor Mat, 142 (2011) 423-438.
[13] J. Weitkamp, Zeolites and catalysis, Solid State Ionics, 131 (2000) 175-188.
[14] W. Vermeiren, J.P. Gilson, Impact of Zeolites on the Petroleum and Petrochemical Industry, Top Catal, 52 (2009) 1131-1161.
[15] A. de Reviere, B. Jacobs, I. Stals, J. De Clercq, Cross-curricular project-based laboratory learning enables hands-on interdisciplinary education for chemical engineering students, Education for Chemical Engineers, 47 (2024) 1-9.
[16] B.O. Hincapie, L.J. Garces, Q. Zhang, A. Sacco, S.L. Suib, Synthesis of mordenite nanocrystals, Micropor Mesopor Mat, 67 (2004) 19-26.
[17] C. Fernandez, I. Stan, J.-P. Gilson, K. Thomas, A. Vicente, A. Bonilla, J. Pérez-Ramírez, Hierarchical ZSM-5 Zeolites in Shape-Selective Xylene Isomerization: Role of Mesoporosity and Acid Site Speciation, Chemistry – A European Journal, 16 (2010) 6224-6233.
[18] W. Song, R.E. Justice, C.A. Jones, V.H. Grassian, S.C. Larsen, Synthesis, Characterization, and Adsorption Properties of Nanocrystalline ZSM-5, Langmuir, 20 (2004) 8301-8306.
[19] G. Reding, T. Maurer, B. Kraushaar-Czarnetzki, Comparing synthesis routes to nano-crystalline zeolite ZSM-5, Micropor Mesopor Mat, 57 (2003) 83-92.

[20] J. Shao, T. Fu, Q. Ma, Z. Ma, C. Zhang, Z. Li, Controllable synthesis of nano-ZSM-5 catalysts with large amount and high strength of acid sites for conversion of methanol to hydrocarbons, Micropor Mesopor Mat, 273 (2019) 122-132.
[21] A. de Reviere, T. Vandevyvere, M. Sabbe, A. Verberckmoes, Renewable Butene Production through Dehydration Reactions over Nano-HZSM-5/γ-Al2O3 Hybrid Catalysts, Catalysts, 10 (2020) 879.
[22] R. Jain, Z. Niu, M. Choudhary, H. Bourji, J.C. Palmer, J.D. Rimer, In Situ Imaging of Faujasite Surface Growth Reveals Unique Pathways of Zeolite Crystallization, J Am Chem Soc, 145 (2023) 1155-1164.
[23] T. Li, F. Krumeich, J.A. van Bokhoven, Where Does the Zeolite ZSM-5 Nucleation and Growth Start? The Effect of Aluminum, Crystal Growth & Design, 19 (2019) 2548-2551.
[24] R.W. Broach, E.P. Boldingh, D.-Y. Jan, G.J. Lewis, J.G. Moscoso, J.C. Bricker, Tailoring zeolite morphology by Charge Density Mismatch for aromatics processing, J Catal, 308 (2013) 142-153.
[25] G. Bellussi, R. Millini, Background and Recent Advances in Ti-Containing Zeolite Materials, in: J. Pérez Pariente, M. Sánchez-Sánchez (Eds.) Structure and Reactivity of Metals in Zeolite Materials, Springer International Publishing, Cham, 2018, pp. 1-52.
[26] Z. Qin, L. Pinard, M.A. Benghalem, T.J. Daou, G. Melinte, O. Ersen, S. Asahina, J.-P. Gilson, V. Valtchev, Preparation of Single-Crystal “House-of-Cards”-like ZSM-5 and Their Performance in Ethanol-to-Hydrocarbon Conversion, Chemistry of Materials, 31 (2019) 4639-4648.
[27] D.M. Roberge, H. Hausmann, W.F. Hölderich, Dealumination of zeolite beta by acid leaching: a new insight with two-dimensional multi-quantum and cross polarization 27Al MAS NMR, Phys Chem Chem Phys, 4 (2002) 3128-3135.
[28] S. van Donk, A.H. Janssen, J.H. Bitter, K.P. de Jong, Generation, Characterization, and Impact of Mesopores in Zeolite Catalysts, Catalysis Reviews, 45 (2003) 297-319.
[29] S. Abelló, A. Bonilla, J. Pérez-Ramírez, Mesoporous ZSM-5 zeolite catalysts prepared by desilication with organic hydroxides and comparison with NaOH leaching, Applied Catalysis A: General, 364 (2009) 191-198.
[30] J.C. Groen, J.C. Jansen, J.A. Moulijn, J. Pérez-Ramírez, Optimal Aluminum-Assisted Mesoporosity Development in MFI Zeolites by Desilication, The Journal of Physical Chemistry B, 108 (2004) 13062-13065.
[31] Z. Qin, G. Melinte, J.-P. Gilson, M. Jaber, K. Bozhilov, P. Boullay, S. Mintova, O. Ersen, V. Valtchev, The Mosaic Structure of Zeolite Crystals, Angewandte Chemie International Edition, 55 (2016) 15049-15052.
[32] Z. Qin, S. Zeng, G. Melinte, T. Bučko, M. Badawi, Y. Shen, J.-P. Gilson, O. Ersen, Y. Wei, Z. Liu, X. Liu, Z. Yan, S. Xu, V. Valtchev, S. Mintova, Understanding the Fundamentals of Microporosity Upgrading in Zeolites: Increasing Diffusion and Catalytic Performances, Advanced Science, 8 (2021) 2100001.
[33] Z. Qin, J.-P. Gilson, V. Valtchev, Mesoporous zeolites by fluoride etching, Current Opinion in Chemical Engineering, 8 (2015) 1-6.
[34] Z. Qin, L. Lakiss, J.P. Gilson, K. Thomas, J.M. Goupil, C. Fernandez, V. Valtchev, Chemical Equilibrium Controlled Etching of MFI-Type Zeolite and Its Influence on Zeolite Structure, Acidity, and Catalytic Activity, Chemistry of Materials, 25 (2013) 2759-2766.
[35] Z. Qin, K.A. Cychosz, G. Melinte, H. El Siblani, J.-P. Gilson, M. Thommes, C. Fernandez, S. Mintova, O. Ersen, V. Valtchev, Opening the Cages of Faujasite-Type Zeolite, J Am Chem Soc, 139 (2017) 17273-17276.

[36] D. Zhang, R. Wang, X. Yang, Effect of P Content on the Catalytic Performance of P-modified HZSM-5 Catalysts in Dehydration of Ethanol to Ethylene, Catal Lett, 124 (2008) 384-391.
[37] S.A. Yashnik, Z.R. Ismagilov, V.F. Anufrienko, Catalytic properties and electronic structure of copper ions in Cu-ZSM-5, Catalysis Today, 110 (2005) 310-322.
[38] D. Verboekend, J. Perez-Ramirez, Design of hierarchical zeolite catalysts by desilication, Catal Sci Technol, 1 (2011) 879-890.
[39] H. Wu, M. Liu, W. Tan, K. Hou, A. Zhang, Y. Wang, X. Guo, Effect of ZSM-5 zeolite morphology on the catalytic performance of the alkylation of toluene with methanol, Journal of Energy Chemistry, 23 (2014) 491-497.
[40] A. Liutkova, H. Zhang, J.F.M. Simons, B. Mezari, M. Mirolo, G.A. Garcia, E.J.M. Hensen, N. Kosinov, Ca Cations Impact the Local Environment inside HZSM-5 Pores during the Methanol-to-Hydrocarbons Reaction, ACS Catalysis, 13 (2023) 3471-3484.
[41] I.S. Yakovleva, S.P. Banzaraktsaeva, E.V. Ovchinnikova, V.A. Chumachenko, L.A. Isupova, Catalytic Dehydration of Bioethanol to Ethylene, Catalysis in Industry, 8 (2016) 152-167.
[42] T.K. Phung, L. Proietti Hernández, A. Lagazzo, G. Busca, Dehydration of ethanol over zeolites, silica alumina and alumina: Lewis acidity, Brønsted acidity and confinement effects, Applied Catalysis A: General, 493 (2015) 77-89.
[43] J. Sun, Y. Wang, Recent Advances in Catalytic Conversion of Ethanol to Chemicals, Acs Catalysis, 4 (2014) 1078-1090.
[44] A. de Reviere, D. Gunst, M. Sabbe, A. Verberckmoes, Sustainable short-chain olefin production through simultaneous dehydration of mixtures of 1-butanol and ethanol over HZSM-5 and γ-Al2O3, Journal of Industrial and Engineering Chemistry, 89 (2020) 257-272.
[45] M. John, K. Alexopoulos, M.F. Reyniers, G.B. Marin, First-Principles Kinetic Study on the Effect of the Zeolite Framework on 1-Butanol Dehydration, ACS Catalysis, 6 (2016) 4081-4094.
[46] A. de Reviere, D. Gunst, M.K. Sabbe, M.-F. Reyniers, A. Verberckmoes, Dehydration of butanol towards butenes over MFI, FAU and MOR: influence of zeolite topology, Catal Sci Technol, (2021).
[47] S. Kumar, A.K. Sinha, S.G. Hegde, S. Sivasanker, Influence of mild dealumination on physicochemical, acidic and catalytic properties of H-ZSM-5, Journal of Molecular Catalysis A: Chemical, 154 (2000) 115-120.
[48] E. Loeffler, U. Lohse, C. Peuker, G. Oehlmann, L.M. Kustov, V.L. Zholobenko, V.B. Kazansky, Study of different states of nonframework aluminum in hydrothermally dealuminated HZSM-5 zeolites using diffuse reflectance i.r. spectroscopy, Zeolites, 10 (1990) 266-271.
[49] R.M. Lago, W.O. Haag, R.J. Mikovsky, D.H. Olson, S.D. Hellring, K.D. Schmitt, G.T. Kerr, The Nature of the Catalytic Sites in HZSM-5- Activity Enhancement, in: Y. Murakami, A. Iijima, J.W. Ward (Eds.) Studies in Surface Science and Catalysis, Elsevier1986, pp. 677-684.
[50] V. Babić, S. Koneti, S. Moldovan, N. Nesterenko, J.-P. Gilson, V. Valtchev, Preparation of hierarchical SSZ-13 by NH4F etching, Micropor Mesopor Mat, 314 (2021) 110863.
[51] J. Rouquerol, P. Llewellyn, F. Rouquerol, Is the bet equation applicable to microporous adsorbents?, in: P.L. Llewellyn, F. Rodriquez-Reinoso, J. Rouqerol, N. Seaton (Eds.) Studies in Surface Science and Catalysis, Elsevier2007, pp. 49-56.
[52] A. Galarneau, F. Villemot, J. Rodriguez, F. Fajula, B. Coasne, Validity of the t-plot Method to Assess Microporosity in Hierarchical Micro/Mesoporous Materials, Langmuir, 30 (2014) 13266-13274.

[53] J.C. Groen, L.A.A. Peffer, J. Pérez-Ramírez, Pore size determination in modified micro- and mesoporous materials. Pitfalls and limitations in gas adsorption data analysis, Micropor Mesopor Mat, 60 (2003) 1-17.
[54] N.S. Nesterenko, F. Thibault-Starzyk, V. Montouilliout, V.V. Yushchenko, C. Fernandez, J.P. Gilson, F. Fajula, I.I. Ivanova, The use of the consecutive adsorption of pyridine bases and carbon monoxide in the IR spectroscopic study of the accessibility of acid sites in microporous/mesoporous materials, Kinetics and Catalysis, 47 (2006) 40-48.
[55] F. Thibault-Starzyk, I. Stan, S. Abelló, A. Bonilla, K. Thomas, C. Fernandez, J.-P. Gilson, J. Pérez-Ramírez, Quantification of enhanced acid site accessibility in hierarchical zeolites – The accessibility index, J Catal, 264 (2009) 11-14.
[56] J.G.M. Winkelman, G.N. Kraai, H.J. Heeres, Binary, ternary and quaternary liquid–liquid equilibria in 1-butanol, oleic acid, water and n-heptane mixtures, Fluid Phase Equilibria, 284 (2009) 71-79.
[57] R.J. Berger, E.H. Stitt, G.B. Marin, F. Kapteijn, J.A. Moulijn, Eurokin - Chemical reaction kinetics in practice, Cattech, 5 (2001) 30-60.
[58] D. Gunst, K. Alexopoulos, K. Van der Borght, M. John, V. Galvita, M.F. Reyniers, A. Verberckmoes, Study of butanol conversion to butenes over H-ZSM-5: Effect of chemical structure on activity, selectivity and reaction pathways, Applied Catalysis A: General, 539 (2017) 1-12.
[59] M. John, K. Alexopoulos, M.F. Reyniers, G.B. Marin, Reaction path analysis for 1-butanol dehydration in H-ZSM-5 zeolite: Ab initio and microkinetic modeling, J. Catal., 330 (2015) 28-45.
[60] M. John, K. Alexopoulos, M.F. Reyniers, G.B. Marin, Mechanistic insights into the formation of butene isomers from 1-butanol in H-ZSM-5: DFT based microkinetic modelling, Catal Sci Technol, 7 (2017) 1055-1072.
[61] D. Gunst, M. Sabbe, M.-F. Reyniers, A. Verberckmoes, Study of n-butanol conversion to butenes: Effect of Si/Al ratio on activity, selectivity and kinetics, Applied Catalysis A: General, 582 (2019) 117101.
[62] A.C. Hindmarsh, ODEPACK, A Systematized Collection of ODE Solvers, in: R.S. Stepleman (Ed.) Scientific Computing, North-Holland, Amsterdam, 1983, pp. 55-64.
[63] K.N. Bozhilov, T.T. Le, Z. Qin, T. Terlier, A. Palčić, J.D. Rimer, V. Valtchev, Time-resolved dissolution elucidates the mechanism of zeolite MFI crystallization, Science Advances, 7 (2021) eabg0454.
[64] Z. Qin, L. Hafiz, Y. Shen, S.V. Daele, P. Boullay, V. Ruaux, S. Mintova, J.-P. Gilson, V. Valtchev, Defect-engineered zeolite porosity and accessibility, Journal of Materials Chemistry A, 8 (2020) 3621-3631.
[65] G. Majano, A. Darwiche, S. Mintova, V. Valtchev, Seed-Induced Crystallization of Nanosized Na-ZSM-5 Crystals, Ind Eng Chem Res, 48 (2009) 7084-7091.
[66] J. Hedlund, M. Zhou, A. Faisal, O.G.W. Öhrman, V. Finelli, M. Signorile, V. Crocellà, M. Grahn, Controlling diffusion resistance, selectivity and deactivation of ZSM-5 catalysts by crystal thickness and defects, J Catal, 410 (2022) 320-332.
[67] J. Holzinger, P. Beato, L.F. Lundegaard, J. Skibsted, Distribution of Aluminum over the Tetrahedral Sites in ZSM-5 Zeolites and Their Evolution after Steam Treatment, The Journal of Physical Chemistry C, 122 (2018) 15595-15613.
[68] L. Rodríguez-González, F. Hermes, M. Bertmer, E. Rodríguez-Castellón, A. Jiménez-López, U. Simon, The acid properties of H-ZSM-5 as studied by NH3-TPD and 27Al-MAS-NMR spectroscopy, Applied Catalysis A: General, 328 (2007) 174-182.

[69] K. Barbera, F. Bonino, S. Bordiga, T.V.W. Janssens, P. Beato, Structure–deactivation relationship for ZSM-5 catalysts governed by framework defects, J Catal, 280 (2011) 196-205.
[70] I.C. Medeiros-Costa, E. Dib, N. Nesterenko, J.-P. Dath, J.-P. Gilson, S. Mintova, Silanol defect engineering and healing in zeolites: opportunities to fine-tune their properties and performances, Chemical Society Reviews, 50 (2021) 11156-11179.
[71] K.S. Triantafyllidis, L. Nalbandian, P.N. Trikalitis, A.K. Ladavos, T. Mavromoustakos, C.P. Nicolaides, Structural, compositional and acidic characteristics of nanosized amorphous or partially crystalline ZSM-5 zeolite-based materials, Micropor Mesopor Mat, 75 (2004) 89-100.
[72] T. Onfroy, Z. Qin, S. Casale, V. Valtchev, Optimization of ammonium fluoride route to hierarchical ZSM-5 zeolites, Micropor Mesopor Mat, 362 (2023) 112760.
[73] R. Khare, Z. Liu, Y. Han, A. Bhan, A mechanistic basis for the effect of aluminum content on ethene selectivity in methanol-to-hydrocarbons conversion on HZSM-5, J Catal, 348 (2017) 300-305.
[74] F. Thibault-Starzyk, A. Vimont, J.-P. Gilson, 2D-COS IR study of coking in xylene isomerisation on H-MFI zeolite, Catalysis Today, 70 (2001) 227-241.
[75] H. Li, J. Yu, K. Du, W. Li, L. Ding, W. Chen, S. Xie, Y. Zhang, Y. Tang, Synthesis of ZSM-5 Zeolite Nanosheets with Tunable Silanol Nest Contents across an Ultra-wide pH Range and Their Catalytic Validation, Angewandte Chemie International Edition, n/a (2024) e202405092.
[76] L. Lakiss, F. Ngoye, C. Canaff, S. Laforge, Y. Pouilloux, Z. Qin, M. Tarighi, K. Thomas, V. Valtchev, A. Vicente, L. Pinard, J.-P. Gilson, C. Fernandez, On the remarkable resistance to coke formation of nanometer-sized and hierarchical MFI zeolites during ethanol to hydrocarbons transformation, J Catal, 328 (2015) 165-172.
[77] R.M. Ravenelle, F. Schüβler, A. D'Amico, N. Danilina, J.A. van Bokhoven, J.A. Lercher, C.W. Jones, C. Sievers, Stability of Zeolites in Hot Liquid Water, The Journal of Physical Chemistry C, 114 (2010) 19582-19595.
[78] K. Alexopoulos, M. John, K. Van der Borght, V. Galvita, M.-F. Reyniers, G.B. Marin, DFT-based microkinetic modeling of ethanol dehydration in H-ZSM-5, J Catal, 339 (2016) 173-185.
[79] M. John, K. Alexopoulos, M.F. Reyniers, G.B. Marin, Reaction path analysis for 1-butanol dehydration in H-ZSM-5 zeolite: Ab initio and microkinetic modeling, J Catal, 330 (2015) 28-45.
[80] Z. Qin, L. Lakiss, L. Tosheva, J.-P. Gilson, A. Vicente, C. Fernandez, V. Valtchev, Comparative Study of Nano-ZSM-5 Catalysts Synthesized in OH− and F− Media, Advanced Functional Materials, 24 (2014) 257-264.
[81] K. Lee, S. Lee, Y. Jun, M. Choi, Cooperative effects of zeolite mesoporosity and defect sites on the amount and location of coke formation and its consequence in deactivation, J Catal, 347 (2017) 222-230.
[82] J. Valecillos, G. Elordi, A.T. Aguayo, P. Castaño, The intrinsic effect of co-feeding water on the formation of active/deactivating species in the methanol-to-hydrocarbons reaction on ZSM-5 zeolite, Catal Sci Technol, 11 (2021) 1269-1281.
[83] H. An, F. Zhang, Z. Guan, X. Liu, F. Fan, C. Li, Investigating the Coke Formation Mechanism of H-ZSM-5 during Methanol Dehydration Using Operando UV–Raman Spectroscopy, ACS Catalysis, 8 (2018) 9207-9215.
[84] B.A. De Moor, M.-F. Reyniers, O.C. Gobin, J.A. Lercher, G.B. Marin, Adsorption of C2−C8 n-Alkanes in Zeolites, The Journal of Physical Chemistry C, 115 (2011) 1204-1219.
[85] A. Farzaneh, R.F. DeJaco, L. Ohlin, A. Holmgren, J.I. Siepmann, M. Grahn, Comparative Study of the Effect of Defects on Selective Adsorption of Butanol from Butanol/Water Binary Vapor Mixtures in Silicalite-1 Films, Langmuir, 33 (2017) 8420-8427.

[86] D.W. Breck, G.W. Skeels, Silicon substituted zeolite compositions and process for preparing same, Google Patents, 1985.